Frontiers of Information Technology & Electronic Engineering
www.jzus.zju.edu.cn; engineering.cae.cn; www.springerlink.com
ISSN 2095-9184 (print); ISSN 2095-9230 (online)
E-mail: jzus@zju.edu.cn

Data-driven intermittent connection fault diagnosis for complex topology DeviceNet based on Bayesian inference*

Longkai WANG, Yong LEI‡

State Key Laboratory of Fluid Power and Mechatronic Systems, Zhejiang University, Hangzhou 310027, China

E-mail: lkwang@zju.edu.cn; ylei@zju.edu.cn

Received Aug. 8, 2024; Revision accepted Nov. 11, 2024; Crosschecked June 17, 2025

Abstract: As the topology of DeviceNet in industrial automation systems grows more complex and the reliability requirement for industrial equipment and processes becomes more stringent, the importance of network troubleshooting is increasingly evident. Intermittent connection (IC) faults frequently occur in DeviceNet systems, impairing production performance and even operational safety. However, existing IC troubleshooting methods for DeviceNet, especially those with complex topologies, cannot directly handle multi-fault scenarios, which require human intervention for a full diagnosis. In this paper, a novel data-driven IC fault diagnosis method based on Bayesian inference is proposed for DeviceNet with complex topologies, which can accurately and efficiently localize all IC faults in the network without interrupting the normal system operation. First, the observation symptoms are defined by analyzing the data frames interrupted by IC faults, and the suspected IC faults are derived by integrating the observation symptoms and the network topology information. Second, a Bayesian inference-based estimation approach for the posterior probability of each suspected fault occurring in the network is proposed using the quantity of observation symptoms and their causal relationships regarding the suspected faults. Finally, a maximum likelihood-based fast diagnosis algorithm is developed to rapidly identify the IC fault locations in various complex scenarios. A laboratory testbed is constructed and case studies are conducted under various topologies and fault scenarios to demonstrate the effectiveness and advantages of the proposed method. Experimental results show that the IC fault locations diagnosed by the proposed method agree well with the experimental setup.

Key words: DeviceNet; Fieldbus; Complex topology; Fault diagnosis; Intermittent connection; Bayesian inference
https://doi.org/10.1631/FITEE.2400696 **CLC number:** TP277

1 Introduction

DeviceNet, a fieldbus network using the controller area network (CAN) as the physical and data link layer protocol (Open DeviceNet Vendor Association, 2021), is widely used for transmitting important data in industrial automation systems, such as automotive manufacturing systems and distributed control systems (Gessner et al., 2014; Cheng et al., 2024a, 2024b), which require excellent real-time performance and network reliability. However, in real-world environments, unavoidable factors such as ambient interference, vibration, and loose connectors can lead to frequent intermittent connection (IC) faults in the network. Manifested as intermittent and random disconnections of network cables in short time intervals, IC fault is a common but hard-to-diagnose problem. It can cause transmission delays or even loss of critical messages due to random interruptions in network communications, which may cause system shutdowns and security-related problems. However, it is tremendously challenging to diagnose IC faults in complex topologies, that is, the hierarchical structures that evolve from

‡ Corresponding author
* Project supported by the National Natural Science Foundation of China (No. 52072341)
ORCID: Longkai WANG, https://orcid.org/0000-0003-0865-0836; Yong LEI, https://orcid.org/0000-0003-0235-5203

bus structures by combining multi-port connectors, because the limited available open-style ports of DeviceNet in practice hinder the diagnosability of the subnets inside the complex topology network (Wang LK et al., 2023). Therefore, timely detection and complete diagnosis of IC faults before they cause system-level failures are of great importance for the reliability of complex topological systems.

In the literature, some preliminary studies have been conducted on IC fault diagnosis methods for CAN networks. Zhao and Lei (2012) and Lei et al. (2014b) applied generalized zero inflated Poisson models to describe the IC-induced errors, and used a ranked probability control chart to monitor the error anomalies. However, the localization of IC faults was not addressed. Lei et al. (2014a, 2015) defined two error events corresponding to different IC fault scenarios in CAN networks, and estimated the confidence intervals of the parameters for the error events to diagnose IC faults. However, their approach depends on analog signal analysis at the physical layer, which is not robust. Based on the data link layer information for the IC-induced errors, Zhang et al. (2017) proposed a context-free-grammar-based IC fault localization method, and Zhang et al. (2019) also proposed a tree-based IC fault diagnosis method. However, the diagnostic accuracy of these qualitative diagnosis methods is unsatisfactory in multi-fault cases, because the ability to discriminate between faulty and non-faulty cables is insufficient due to an inability to precisely quantify the possibility of an IC fault. In addition, the above methods are not applicable to general complex topologies, because they have not considered the impact of sensor locations on diagnosability in different network topologies. Wang LK et al. (2023) proposed an IC fault diagnosability analysis method for CAN networks with complex topologies and an IC fault diagnosis approach using a "divide-and-conquer" strategy to ensure complete diagnosability in multi-fault cases. However, this progressive compression strategy is essentially a repeated implementation of the qualitative diagnosis method on the network, which can identify more IC faults but has limited diagnostic accuracy because the precise probabilities of faults occurring on cables are still not estimated to differentiate the failure conditions of each cable.

The data-driven Bayesian approach is an effective tool for accurately quantifying the probability of faults in the fault diagnosis field, which leads to wide applications in multi-fault diagnosis problems (Cai et al., 2017; Jiang et al., 2023; Yang C et al., 2023a, 2023b). For example, Chu et al. (2023) proposed a fault source diagnosis method for small-batch manufacturing processes of complex products using reverse Bayesian inference. Nguyen and Vilim (2023) developed a framework for assessing the probability distributions of faults in nuclear systems using Bayesian inference. Yang WT et al. (2022) proposed an interpretable unsupervised machine learning model for process monitoring and diagnosis based on Bayesian networks. Liu ZK et al. (2022) constructed a fault diagnosis model for rolling element bearings using a Bayesian network. Liu BY et al. (2022) proposed a Bayesian network fault diagnosis method for radar equipment based on the multi-source information fusion technology. Wang ZW et al. (2021) proposed a fault diagnosis method for building energy systems using a fused reference model and a Bayesian network. However, the Bayesian approach has yet to be fully exploited for multi-IC fault diagnosis in DeviceNet and CAN.

As can be seen from the literature, few works have focused on IC fault diagnosis for the complex topology DeviceNet/CAN, and the diagnostic performance of existing IC fault diagnosis methods proposed in the literature (Lei et al., 2014a, 2015; Zhang et al., 2017, 2019; Wang LK et al., 2023) is limited in complex topology scenarios due to the following drawbacks (detailed analysis is presented in the discussion section): First, the localization accuracy of existing methods is limited because their distribution-based qualitative diagnostic strategy cannot correctly diagnose some special locations in the network. Second, the diagnosis efficiency of existing methods is improvable because they require repeatedly deploying sensors and collecting and processing data to diagnose different areas in the network several times. In addition, the data acquisition (DAQ) schemes of existing methods require sensors to be hooked up inside the network, while in practice most of the connectors inside DeviceNet are not open for access, which greatly limits the applicability of these methods in industrial environments. Therefore, there is an urgent need to develop an accurate and efficient IC fault diagnosis method for the complex topology DeviceNet, which can be easily and practically implemented in industrial applications.

In this paper, a novel data-driven fault diagnosis method is proposed to accurately locate the IC faults in the complex topology DeviceNet without interrupting the normal system operation. The advantages of the proposed method are as follows: First, an accurate and efficient data-driven diagnostic framework is designed by formalizing the IC fault location problem as a Bayesian problem for dealing with the fault occurrence probability from symptom data, which can determine the full locations of IC faults in a single diagnosis, whereas existing methods require iterative diagnosis of several areas in the network. Second, a rapid fault localization algorithm based on Bayesian inference of fault likelihoods, generalized to various network topologies, is developed, which has lower computational complexity than existing algorithms and can thus be extended to large industrial systems. Third, this method provides a practical-to-implement DAQ scheme that needs to attach sensors only to the open ports at the network ends to diagnose the entire network, without the need to deploy them at the unreachable network interior as existing methods. The results of this study will promote the comprehensive diagnosis of DeviceNet systems to ensure system reliability and provide practitioners with the optimal repair schedule for faulty components to minimize system maintenance costs.

2 Preliminaries

In this section, the characteristics of IC faults in the complex topology DeviceNet are introduced. Then the issues faced in this work are presented.

2.1 IC faults in complex topology networks

The complex topology DeviceNet is a hybrid tree and bus topology that contains multiple branches. The branches connect multiple nodes and are connected to each other by a coupling point. Fig. 1 shows an example of a complex topology DeviceNet with Q branches, mQ nodes, and c coupling points, where $\mathbb{B}_Q$ denotes the Q^{th} branch, N_{mQ} denotes the $(mQ)^{\text{th}}$ node, b_c denotes the c^{th} coupling point, and the sensor s_k ($k \in \{1, 2, \cdots, z\}$, z is the number of sensors) is introduced in Section 3.1.

The lines directly connecting the nodes are drop lines, on which the IC faults that occur are defined as local IC faults; the other lines are trunk lines, on which the IC faults that occur are defined as trunk IC faults. In this paper, the complex fault scenario refers to the case where two trunk IC faults occur on the same branch, such as the scenario in Fig. 1. The non-diagnosable subnet refers to the subnet between two trunk IC faults occurring on the same branch (Wang LK et al., 2023), which is denoted by SN in Fig. 1.

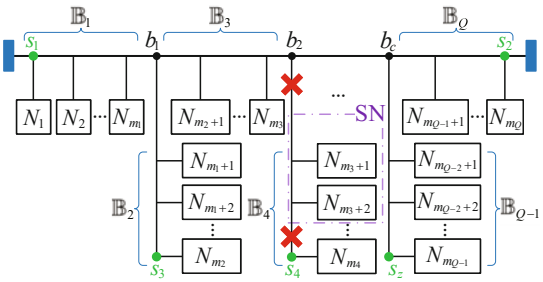

Fig. 1 An example of a complex topology DeviceNet

The lines that suffer from IC faults will be transiently disconnected, and the transmitting dominant bit will turn to the recessive bit at the disconnected location, which will cause incorrect logic bits in some areas of the bus. Any node in the system that detects an error will alert it by sending an error frame to interrupt the transmission of the current data frame.

2.2 Problem definition

In this work, the only condition for diagnosing the complex topology DeviceNet is the error frames induced by the IC faults, which provide very limited diagnostic information. Hence, for locating all IC faults completely, the following issues need to be addressed:

1. How can an error frame be mapped to the possible locations of IC faults?

2. How can the fault probability for each possible location be quantitatively assessed?

3. How can all IC faults in a network, including non-diagnosable subnets, be accurately diagnosed without reconfiguring the sensors?

The assumptions in this work include: (1) The communication lines between the DAQ system and the network are reliable; (2) The IC faults are independent and persistent over time; (3) Without loss of generality, open ports are provided at each end of the network branch for hooking up external equipment.

3 Methodology

This paper proposes a data-driven IC fault diagnosis methodology for the complex topology DeviceNet based on Bayesian inference. The basic idea of this methodology is that each occurrence of an IC fault will increase the number of corresponding symptoms among the nodes, so that the locations of all IC faults in the network can be accurately determined based on the posterior probability of each fault calculated using the number of symptoms.

The framework of the proposed methodology is shown in Fig. 2. Once a frame transmitted on the network is corrupted, the interrupted frame is collected and analyzed to produce a corresponding observation symptom for each node. On one hand, for each observation symptom, the suspected IC faults that may lead to symptom production can be derived based on the network topology information. On the other hand, the likelihood of each suspected fault occurring in the network can be accurately calculated based on Bayesian inference using the quantity information of the observation symptom. After that, on the basis of the observation symptoms of all nodes and their suspected faults, the maximum likelihood-based fast diagnosis (MLBFD) algorithm can be applied to identify the complete location of the IC faults in the network with the help of the likelihood of each fault. Details of the proposed method are introduced in the following subsections.

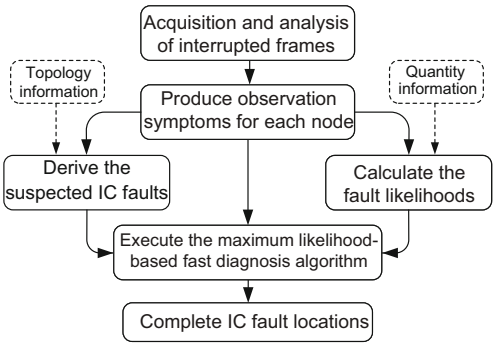

Fig. 2 Framework of the proposed methodology

3.1 Definition of observation symptoms

Field programmable gate array (FPGA)-based sensors $s_k, k \in \{1, 2, \cdots, z\}$, are deployed at all ends of the network to collect the interrupted frame on the data link layer as soon as an error frame occurs, as shown in Fig. 1. The sensors compare each interrupted frame recorded to the normal frame with the same source address. Normal frames can be recorded when the bus is fault-free. As shown in Fig. 3, because the data frame transmitted by N_2 is interrupted by IC faults, the data collected by sensor s_2 are different from the normal frame, and then the false error event $e_{s_2} = \mathbb{F}$ is produced for N_2, which indicates that IC faults occur on $\mathcal{P}_{N_2-s_2}$, where $\mathcal{P}_{N_2-s_2}$ is the communication path between N_2 and s_2. In contrast, the data collected by sensor s_1 are the same as the normal frame, and then the true error event $e_{s_1} = \mathbb{T}$ is produced for N_2, which indicates that $\mathcal{P}_{N_2-s_1}$ is fault-free.

When an IC fault interrupts the transmission of node $N_i, \forall i \in \{1, 2, \cdots, n\}$, the z sensors will produce z error events for N_i, and an observation symptom is produced by sequentially combining these error events. If there are multiple IC faults in the network, there will be multiple interruptions in the transmission of node N_i, and thus the sensor will generate multiple observation symptoms for N_i. The mode of observation symptoms varies with the type and location of the IC faults. Note that a node may not have all 2^z modes of observation symptoms. Assuming that after measurement, node N_i has a total of m_i modes of observation symptoms due to all IC faults, then they can be represented as

$$\begin{cases} \mathfrak{a}_{N_i}^{<1>} = (e_{s_1}^{<1>}, e_{s_2}^{<1>}, \cdots, e_{s_z}^{<1>}), \\ \mathfrak{a}_{N_i}^{<2>} = (e_{s_1}^{<2>}, e_{s_2}^{<2>}, \cdots, e_{s_z}^{<2>}), \\ \quad \vdots \\ \mathfrak{a}_{N_i}^{<m_i>} = (e_{s_1}^{<m_i>}, e_{s_2}^{<m_i>}, \cdots, e_{s_z}^{<m_i>}), \end{cases} \tag{1}$$

where $\mathfrak{a}_{N_i}^{<t>}$ is the t^{th} mode of the observation symptom for node N_i, $\forall t \in \{1, 2, \cdots, m_i\}$, and $e_{s_k}^{<t>}$ is the error event produced by sensor s_k in $\mathfrak{a}_{N_i}^{<t>}$, $\forall k \in \{1, 2, \cdots, z\}$.

3.2 Derivation of the suspected IC faults

Based on the above analysis, each observation symptom for a node contains information about

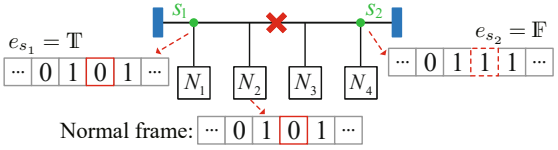

Fig. 3 Illustration of the error events

whether the IC fault has occurred on the communication path between the node and each sensor. Hence, for each observation symptom, a set of suspected IC faults can be derived by combining the observation symptom with the network topology.

In the network, the communication path between node N_i and sensor s_k, i.e., $\mathcal{P}_{N_i-s_k}$, is formed by the logical combination of the links. To facilitate analysis, let $\mathcal{L}_{N_i-s_k}$ denote the set of links that form $\mathcal{P}_{N_i-s_k}$.

For an observation symptom $\mathfrak{a}_{N_i}^{<t>} = (e_{s_1}^{<t>}, e_{s_2}^{<t>}, \cdots, e_{s_z}^{<t>})$, if $e_{s_k}^{<t>} = \mathbb{T}$, then every link in $\mathcal{L}_{N_i-s_k}$ is free of IC faults, and any link other than the links in $\mathcal{L}_{N_i-s_k}$ is suspected to have suffered IC faults. Conversely, if $e_{s_k}^{<t>} = \mathbb{F}$, then any link in $\mathcal{L}_{N_i-s_k}$ is suspected to have suffered IC faults.

Then, $\forall t \in \{1, 2, \cdots, m_i\}$, the set of all suspected IC faults indicated by $\mathfrak{a}_{N_i}^{<t>}$, denoted as $\mathcal{F}_{N_i}^{<t>}$, is the intersection of the analysis results of all error events in $\mathfrak{a}_{N_i}^{<t>}$, that is,

$$\mathcal{F}_{N_i}^{<t>} = \left\{ f_j \middle| j \in \left(\mathcal{L} - \bigcup_{e_{s_k}^{<t>}=\mathbb{T}} \mathcal{L}_{N_i-s_k} \right) \bigcap \left(\bigcap_{e_{s_k}^{<t>}=\mathbb{F}} \mathcal{L}_{N_i-s_k} \right) \right\}, \tag{2}$$

where $\forall k \in \{1, 2, \cdots, z\}$, f_j denotes the suspected IC fault occurring on link j, and $\mathcal{L}$ denotes the set of all links in the network.

3.3 Likelihood of the suspected IC faults

It can be inferred from Section 3.2 that the occurrence of a suspected IC fault will increase only the number of observation symptoms from which it can be derived. Thus, the probability of each suspected IC fault occurring in the network can be calculated by synthesizing the quantity information of observation symptoms.

For further analysis, let $\mathcal{S}_{\mathrm{o}}$ denote the set of sequentially combined observation symptoms of each node, which can be represented as

$$\begin{aligned} \mathcal{S}_{\mathrm{o}} &= \{\mathfrak{a}_{N_1}^{<1>}, \cdots, \mathfrak{a}_{N_1}^{<m_1>}, \mathfrak{a}_{N_2}^{<1>}, \cdots, \mathfrak{a}_{N_2}^{<m_2>}, \\ &\quad \cdots, \mathfrak{a}_{N_n}^{<1>}, \cdots, \mathfrak{a}_{N_n}^{<m_n>}\} \\ &= \{\mathfrak{a}_{\mathrm{o}}^{(1)}, \mathfrak{a}_{\mathrm{o}}^{(2)}, \cdots, \mathfrak{a}_{\mathrm{o}}^{(d)}\}, \end{aligned} \tag{3}$$

where $d = \sum_{q=1}^{n} m_q$ denotes the number of observation symptom modes. $\forall \mathfrak{a}_{\mathrm{o}}^{(v)} \in \mathcal{S}_{\mathrm{o}}$, its corresponding communication path is denoted as $\mathcal{P}_{\mathrm{o}}^{(v)}$, the set of network links composing $\mathcal{P}_{\mathrm{o}}^{(v)}$ is denoted as $\mathcal{L}_{\mathrm{o}}^{(v)}$, and the set of suspected IC faults that occur on links in the set $\mathcal{L}_{\mathrm{o}}^{(v)}$ is denoted as $\mathcal{F}_{\mathrm{o}}^{(v)}$, $\mathcal{F}_{\mathrm{o}}^{(v)} = \{f_1, f_2, \cdots, f_u\}$, where u denotes the number of suspected faults in $\mathcal{F}_{\mathrm{o}}^{(v)}$, $v = 1, 2, \cdots, d$.

Based on the quantity of each observation symptom and the subordination (causal) relationship between f_j and each observation symptom, the probability $\Pr(\mathfrak{a}_{\mathrm{o}}^{(v)}|f_j)$ can be directly calculated as

$$\Pr(\mathfrak{a}_{\mathrm{o}}^{(v)}|f_j) = \frac{\mathcal{Q}(\mathfrak{a}_{\mathrm{o}}^{(v)})}{\sum\limits_{\mathfrak{a}_{\mathrm{o}}^{(c)}: f_j \in \mathcal{F}_{\mathrm{o}}^{(c)}} \mathcal{Q}(\mathfrak{a}_{\mathrm{o}}^{(c)})}, \ \forall f_j \in \bigcup_{v=1}^{d} \mathcal{F}_{\mathrm{o}}^{(v)}, \tag{4}$$

where $\mathcal{Q}(\mathfrak{a}_{\mathrm{o}}^{(v)})$ denotes the quantity of observation symptoms $\mathfrak{a}_{\mathrm{o}}^{(v)}$.

In this work, $\mathfrak{C}_{f_j}$ denotes the likelihood of f_j, which represents the confidence that the suspected IC fault f_j occurs in the network and is calculated by

$$\mathfrak{C}_{f_j} = \frac{1}{d} \sum_{v=1}^{d} \Pr(f_j|\mathfrak{a}_{\mathrm{o}}^{(v)}), \tag{5}$$

where the posterior probability of all $f_j \in \bigcup_{v=1}^{d} \mathcal{F}_{\mathrm{o}}^{(v)}$ can be calculated using Bayes' formula, that is,

$$\Pr(f_j|\mathfrak{a}_{\mathrm{o}}^{(v)}) = \frac{\Pr(\mathfrak{a}_{\mathrm{o}}^{(v)}|f_j)\Pr(f_j)}{\sum_{i=1}^{u} \Pr(\mathfrak{a}_{\mathrm{o}}^{(v)}|f_i)\Pr(f_i)}. \tag{6}$$

Here, the prior probability $\Pr(f_j)$ can be estimated by solving the following constrained optimization problem for the difference between the fitted probability and the actual probability of the observation symptoms:

$$\begin{cases} \min\limits_{\Pr(f_j): f_j \in \bigcup\limits_{v=1}^{d} \mathcal{F}_{\mathrm{o}}^{(v)}} \sum\limits_{v=1}^{d} \left| \hat{\Pr}(\mathfrak{a}_{\mathrm{o}}^{(v)}) - \Pr(\mathfrak{a}_{\mathrm{o}}^{(v)}) \right|^2 \ \text{s.t.} \\ \hat{\Pr}(\mathfrak{a}_{\mathrm{o}}^{(v)}) = \sum\limits_{i=1}^{u} \Pr(\mathfrak{a}_{\mathrm{o}}^{(v)}|f_i)\Pr(f_i), \\ \Pr(\mathfrak{a}_{\mathrm{o}}^{(v)}) = \dfrac{\mathcal{Q}(\mathfrak{a}_{\mathrm{o}}^{(v)})}{\sum\limits_{x=1}^{d} \mathcal{Q}(\mathfrak{a}_{\mathrm{o}}^{(x)})}, \ 0 \le \Pr(f_j) \le 1. \end{cases} \tag{7}$$

3.4 Maximum likelihood-based fast diagnosis algorithm

The MLBFD algorithm determines all locations of IC faults by selecting suspected IC faults in descending order of their likelihoods to explain the observation symptoms, until $\mathcal{S}_{\mathrm{o}}$ is completely covered, as shown in Algorithm 1, where $F_{\max}$ is the set of suspected IC faults with the highest likelihood. Let $\mathcal{S}_{\mathrm{R}}$ denote the set of observation symptoms remaining to be explained, F_{R} denote the set of suspected IC faults that may cause $\mathcal{S}_{\mathrm{R}}$, and $\mathcal{S}_{f_j}$ denote the set of observation symptoms that can be explained by f_j, which can be derived by $\mathcal{S}_{f_j}=\bigcup_{v=1}^{d}\{\mathfrak{a}_{f_j}^{(v)}\}$, where $\{\mathfrak{a}_{f_j}^{(v)}\}$ is subjected to Eq. (8) and $\mathfrak{a}_{\mathrm{o}}^{(v)}\in\mathcal{S}_{\mathrm{o}}$.

$$\{\mathfrak{a}_{f_j}^{(v)}\}=\begin{cases}\{\mathfrak{a}_{\mathrm{o}}^{(v)}\}, & \text{if } f_j\in\mathcal{F}_{\mathrm{o}}^{(v)},\\ \varnothing, & \text{otherwise.}\end{cases}\tag{8}$$

Algorithm 1 Maximum likelihood-based fast diagnosis (MLBFD)

Initialization: $F_{\mathrm{R}}=\bigcup_{\mathfrak{a}_{\mathrm{o}}^{(v)}\in\mathcal{S}_{\mathrm{o}}}\mathcal{F}_{\mathrm{o}}^{(v)}$, $\mathcal{S}_{\mathrm{R}}=\mathcal{S}_{\mathrm{o}}$, $\mathcal{H}=\varnothing$

MLBFD($F_{\mathrm{R}},\mathcal{S}_{\mathrm{R}}$):

for all $f_j\in F_{\mathrm{R}}$ **do**
  $F_{\max}\leftarrow\varnothing$
  if $\mathfrak{C}_{f_j}$ is maximum **then**
    $F_{\max}\leftarrow F_{\max}\bigcup\{f_j\}$
  end if
end for
for all $f_j\in F_{\max}$ **do**
  $\mathcal{H}\leftarrow\mathcal{H}\bigcup\{f_j\}$
  $\mathcal{S}_{\mathrm{R}}\leftarrow\mathcal{S}_{\mathrm{R}}-\bigcup_{f_j\in\mathcal{H}}\mathcal{S}_{f_j}$
  if $\mathcal{S}_{\mathrm{R}}=\varnothing$ **then**
    return $\mathcal{H}$
  else
    $F_{\mathrm{R}}\leftarrow\bigcup_{\mathfrak{a}_{\mathrm{o}}^{(v)}\in\mathcal{S}_{\mathrm{R}}}\mathcal{F}_{\mathrm{o}}^{(v)}$
    return MLBFD($F_{\mathrm{R}},\mathcal{S}_{\mathrm{R}}$)
  end if
end for

Initially, the set of observation symptoms remaining to be explained is $\mathcal{S}_{\mathrm{o}}$, F_{R} is the concatenated set of suspected IC faults corresponding to each element in $\mathcal{S}_{\mathrm{o}}$, and the set of determined IC faults $\mathcal{H}$ is initialized to an empty set. Then, the recursive step MLBFD($F_{\mathrm{R}},\mathcal{S}_{\mathrm{R}}$) is defined, and the suspected IC fault with the highest likelihood is selected from F_{R}. Next, each selected suspected IC fault is promoted to a determined IC fault, and the set of observation symptoms that can be explained by the determined IC fault is deleted from $\mathcal{S}_{\mathrm{R}}$. If $\mathcal{S}_{\mathrm{R}}$ is an empty set, the elements in $\mathcal{H}$ are the complete locations of IC faults in the network because they can explain the whole $\mathcal{S}_{\mathrm{o}}$; otherwise, update F_{R} and call the recursive step MLBFD($F_{\mathrm{R}},\mathcal{S}_{\mathrm{R}}$).

Because the MLBFD algorithm uses the exact posterior probability of each suspected IC fault for logical judgment, unlike the algorithm in Wang LK et al. (2023), which uses the partially same qualitative fault probabilities, the computational complexity of the MLBFD algorithm is lower than that of the algorithm in Wang LK et al. (2023). Details of the analysis of the algorithm complexity and the comparison with existing algorithms are presented in the discussion section.

4 Experiments

To demonstrate the effectiveness and improvements of the proposed methodology, a testbed is constructed and three case studies are conducted. In case study 1, the diagnostic procedure is demonstrated in detail using a simple topology network. In case study 2, the effectiveness of the proposed method for diagnosing a complex topology is illustrated. In case study 3, the universality of the proposed method for different topologies is verified.

Fig. 4 shows the constructed testbed, which contains three modules: DeviceNet communication system, IC fault injection system, and error acquisition system. The communication system is constructed using Rockwell AB DeviceNet modules, and the communication speed is set at 500 kb/s. The IC fault injection system contains the LabVIEW program on a personal computer (PC), the NI CRIO controller, and analog switches. The IC faults are injected on a cable using an analog switch whose high-speed on-off is controlled by a PC program through the NI CRIO controller. Multiple IC faults on different cables are

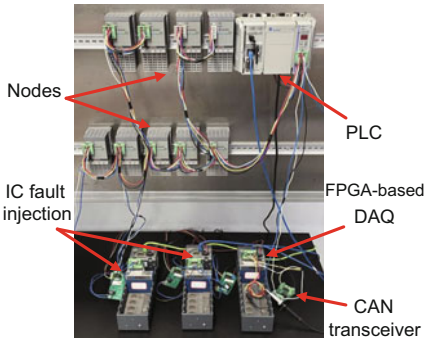

Fig. 4 The testbed constructed for case studies

injected by different switches simultaneously. Each switch is controlled independently, the duration of a cable disconnection event is set to be half bit (1 μs), and the arrivals of the cable disconnection events follow a Poisson process with the arrival rate of an IC fault λ_{IC}. Note that the emulated faults do not lose the intermittency property under accelerated conditions because the duration is sufficiently short. The error acquisition system records fault information based on the NI CRIO FPGA DAQ framework.

4.1 Case study 1: IC fault diagnosis for a simple topology network

The network topology used in this case study is shown in Fig. 5, where two sensors s_1 and s_2 are deployed at both ends of the bus. IC faults are independently injected into five cables: l_{15} has local IC faults at an injection rate of $\lambda_{\mathrm{IC}}^{l_{15}} = 1000$ faults per second (faults/s), and l_1, l_3, l_7, and l_9 have trunk IC faults at injection rates of $\lambda_{\mathrm{IC}}^{l_1} = 300$, $\lambda_{\mathrm{IC}}^{l_3} = 500$, $\lambda_{\mathrm{IC}}^{l_7} = 667$, and $\lambda_{\mathrm{IC}}^{l_9} = 250$ faults/s. A total of 1666 error records are received in this case study.

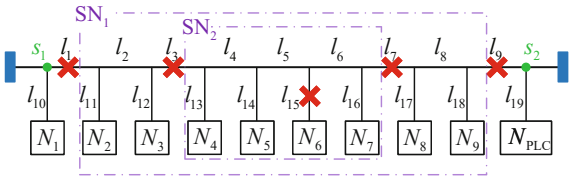

Fig. 5 Experimental setup in case study 1

The significant modes of the observation symptoms for all nodes as well as their quantities are shown in Table 1. Then, the set of observation symptoms can be expressed as $\mathcal{S}_{\mathrm{o}} = \{\mathfrak{a}_{N_1}^{<1>}, \mathfrak{a}_{N_1}^{<2>}, \mathfrak{a}_{N_2}^{<1>}, \cdots, \mathfrak{a}_{N_{\mathrm{PLC}}}^{<2>}\} = \{\mathfrak{a}_{\mathrm{o}}^{(u)} | u \in \{1, 2, \cdots, 28\}\}$.

Step 1: derive the set of suspected IC faults $\mathcal{F}_{\mathrm{o}}^{(u)}$ ($u \in \{1, 2, \cdots, 28\}$) for the corresponding observation symptom $\mathfrak{a}_{\mathrm{o}}^{(u)}$ by Eq. (2), as shown in Table 2.

Step 2: calculate the likelihood of all $f_j \in \bigcup_{v=1}^{28} \mathcal{F}_{\mathrm{o}}^{(v)}$ by Eq. (5), as shown in Table 3.

Step 3: determine the IC fault locations using Algorithm 1. The algorithm execution process is illustrated in Fig. 6, and details are presented as follows:

Recursion 1: $\mathcal{S}_{\mathrm{R}} = \mathcal{S}_{\mathrm{o}}$ and $F_{\mathrm{R}} = \bigcup_{\mathfrak{a}_{\mathrm{o}}^{(u)} \in \mathcal{S}_{\mathrm{R}}} \mathcal{F}_{\mathrm{o}}^{(u)} = \{f_{l_1}, f_{l_2}, \cdots, f_{l_{19}}\}$. $\mathfrak{C}_{f_{l_{15}}}$ is the maximum likelihood, $f_{l_{15}}$ is promoted to the determined IC fault, and $\mathcal{H} = \{f_{l_{15}}\}$. Delete the observation symptoms explained by $f_{l_{15}}$ from $\mathcal{S}_{\mathrm{R}}$. Thus, $\mathcal{S}_{\mathrm{R}} = \{\mathfrak{a}_{\mathrm{o}}^{(u)} | u \in \{2, 4, 5, 7, 8, 10, 11, 13, 14, 16, 17, 19, 20, 22, 23, 25, 26, 28\}\}$.

Table 1 Modes of observation symptoms and the corresponding quantities in case study 1

N_i	$t=1$		$t=2$		$t=3$	
	$\mathfrak{a}_{N_i}^{<t>}$	$\mathcal{Q}(\mathfrak{a}_{N_i}^{<t>})$	$\mathfrak{a}_{N_i}^{<t>}$	$\mathcal{Q}(\mathfrak{a}_{N_i}^{<t>})$	$\mathfrak{a}_{N_i}^{<t>}$	$\mathcal{Q}(\mathfrak{a}_{N_i}^{<t>})$
N_1	$(\mathbb{T}, \mathbb{T})$	44	$(\mathbb{T}, \mathbb{F})$	95	–	–
N_2	$(\mathbb{T}, \mathbb{T})$	35	$(\mathbb{T}, \mathbb{F})$	41	$(\mathbb{F}, \mathbb{T})$	10
N_3	$(\mathbb{T}, \mathbb{T})$	32	$(\mathbb{T}, \mathbb{F})$	64	$(\mathbb{F}, \mathbb{T})$	17
N_4	$(\mathbb{T}, \mathbb{T})$	27	$(\mathbb{T}, \mathbb{F})$	45	$(\mathbb{F}, \mathbb{T})$	41
N_5	$(\mathbb{T}, \mathbb{T})$	57	$(\mathbb{T}, \mathbb{F})$	57	$(\mathbb{F}, \mathbb{T})$	50
N_6	$(\mathbb{F}, \mathbb{F})$	33	$(\mathbb{T}, \mathbb{F})$	31	$(\mathbb{F}, \mathbb{T})$	47
N_7	$(\mathbb{T}, \mathbb{T})$	22	$(\mathbb{T}, \mathbb{F})$	35	$(\mathbb{F}, \mathbb{T})$	25
N_8	$(\mathbb{T}, \mathbb{T})$	16	$(\mathbb{T}, \mathbb{F})$	8	$(\mathbb{F}, \mathbb{T})$	44
N_9	$(\mathbb{T}, \mathbb{T})$	18	$(\mathbb{T}, \mathbb{F})$	9	$(\mathbb{F}, \mathbb{T})$	31
N_{PLC}	$(\mathbb{T}, \mathbb{T})$	201	$(\mathbb{F}, \mathbb{T})$	464	–	–

"–" denotes that the corresponding observation symptom is not significant

Recursion 2: update $F_{\mathrm{R}} = \bigcup_{\mathfrak{a}_{\mathrm{o}}^{(u)} \in \mathcal{S}_{\mathrm{R}}} \mathcal{F}_{\mathrm{o}}^{(u)} = \{f_{l_1}, f_{l_2}, \cdots, f_{l_9}\}$. $\mathfrak{C}_{f_{l_7}}$ is the maximum likelihood, and thus $\mathcal{H} = \{f_{l_{15}}, f_{l_7}\}$ is updated. Delete the observation symptoms explained by f_{l_7} from $\mathcal{S}_{\mathrm{R}}$. Thus, $\mathcal{S}_{\mathrm{R}} = \{\mathfrak{a}_{\mathrm{o}}^{(u)} | u \in \{5, 8, 11, 14, 17, 20, 22, 25\}\}$.

Recursion 3: update $F_{\mathrm{R}} = \bigcup_{\mathfrak{a}_{\mathrm{o}}^{(u)} \in \mathcal{S}_{\mathrm{R}}} \mathcal{F}_{\mathrm{o}}^{(u)} = \{f_{l_1}, f_{l_2}, \cdots, f_{l_6}, f_{l_8}, f_{l_9}\}$. $\mathfrak{C}_{f_{l_3}}$ is the maximum likelihood, and thus $\mathcal{H} = \{f_{l_{15}}, f_{l_7}, f_{l_3}\}$ is updated. Delete the observation symptoms explained by f_{l_3} from $\mathcal{S}_{\mathrm{R}}$. Thus, $\mathcal{S}_{\mathrm{R}} = \{\mathfrak{a}_{\mathrm{o}}^{(u)} | u \in \{5, 8, 22, 25\}\}$.

Recursion 4: update $F_{\mathrm{R}} = \bigcup_{\mathfrak{a}_{\mathrm{o}}^{(u)} \in \mathcal{S}_{\mathrm{R}}} \mathcal{F}_{\mathrm{o}}^{(u)} = \{f_{l_1}, f_{l_2}, f_{l_8}, f_{l_9}\}$. $\mathfrak{C}_{f_{l_9}}$ is the maximum likelihood, and thus $\mathcal{H} = \{f_{l_{15}}, f_{l_7}, f_{l_3}, f_{l_9}\}$ is updated. Delete the observation symptoms explained by f_{l_9} from $\mathcal{S}_{\mathrm{R}}$. Thus, $\mathcal{S}_{\mathrm{R}} = \{\mathfrak{a}_{\mathrm{o}}^{(u)} | u \in \{5, 8\}\}$.

Recursion 5: update $F_{\mathrm{R}} = \bigcup_{\mathfrak{a}_{\mathrm{o}}^{(u)} \in \mathcal{S}_{\mathrm{R}}} \mathcal{F}_{\mathrm{o}}^{(u)} = \{f_{l_1}, f_{l_2}\}$. $\mathfrak{C}_{f_{l_1}}$ is the maximum likelihood, and thus $\mathcal{H} = \{f_{l_{15}}, f_{l_7}, f_{l_3}, f_{l_9}, f_{l_1}\}$ is updated. Delete the observation symptoms explained by f_{l_1} from $\mathcal{S}_{\mathrm{R}}$. Thus, $\mathcal{S}_{\mathrm{R}} = \varnothing$ and the execution ends.

Hence, the determined IC faults are f_{l_1}, f_{l_3}, f_{l_7}, f_{l_9}, and $f_{l_{15}}$, which agrees with the experimental setup.

4.2 Case study 2: IC fault diagnosis for a three-branch complex topology network

In this case study, the network topology is shown in Fig. 7, which has 3 branches connecting 10 nodes. Three sensors s_1, s_2, s_3 are deployed at the ends of

Table 2 Suspected IC fault sets of the corresponding observation symptoms in case study 1

N_i	$\mathcal{F}_{N_i}^{<1>}$	$\mathcal{F}_{N_i}^{<2>}$	$\mathcal{F}_{N_i}^{<3>}$
N_1	$\{f_{l_{11}}, f_{l_{12}}, f_{l_{13}}, f_{l_{14}}, f_{l_{15}}, \cdots, f_{l_{19}}\}$	$\{f_{l_1}, f_{l_2}, f_{l_3}, f_{l_4}, f_{l_5}, f_{l_6}, f_{l_7}, f_{l_8}, f_{l_9}\}$	–
N_2	$\{f_{l_{10}}, f_{l_{12}}, f_{l_{13}}, f_{l_{14}}, f_{l_{15}}, \cdots, f_{l_{19}}\}$	$\{f_{l_2}, f_{l_3}, f_{l_4}, f_{l_5}, f_{l_6}, f_{l_7}, f_{l_8}, f_{l_9}\}$	$\{f_{l_1}\}$
N_3	$\{f_{l_{10}}, f_{l_{11}}, f_{l_{13}}, f_{l_{14}}, f_{l_{15}}, \cdots, f_{l_{19}}\}$	$\{f_{l_3}, f_{l_4}, f_{l_5}, f_{l_6}, f_{l_7}, f_{l_8}, f_{l_9}\}$	$\{f_{l_1}, f_{l_2}\}$
N_4	$\{f_{l_{10}}, f_{l_{11}}, f_{l_{12}}, f_{l_{14}}, f_{l_{15}}, \cdots, f_{l_{19}}\}$	$\{f_{l_4}, f_{l_5}, f_{l_6}, f_{l_7}, f_{l_8}, f_{l_9}\}$	$\{f_{l_1}, f_{l_2}, f_{l_3}\}$
N_5	$\{f_{l_{10}}, f_{l_{11}}, f_{l_{12}}, f_{l_{13}}, f_{l_{15}}, \cdots, f_{l_{19}}\}$	$\{f_{l_5}, f_{l_6}, f_{l_7}, f_{l_8}, f_{l_9}\}$	$\{f_{l_1}, f_{l_2}, f_{l_3}, f_{l_4}\}$
N_6	$\{f_{l_{15}}\}$	$\{f_{l_6}, f_{l_7}, f_{l_8}, f_{l_9}\}$	$\{f_{l_1}, f_{l_2}, f_{l_3}, f_{l_4}, f_{l_5}\}$
N_7	$\{f_{l_{10}}, f_{l_{11}}, \cdots, f_{l_{15}}, f_{l_{17}}, f_{l_{18}}, f_{l_{19}}\}$	$\{f_{l_7}, f_{l_8}, f_{l_9}\}$	$\{f_{l_1}, f_{l_2}, f_{l_3}, f_{l_4}, f_{l_5}, f_{l_6}\}$
N_8	$\{f_{l_{10}}, f_{l_{11}}, \cdots, f_{l_{15}}, f_{l_{16}}, f_{l_{18}}, f_{l_{19}}\}$	$\{f_{l_8}, f_{l_9}\}$	$\{f_{l_1}, f_{l_2}, f_{l_3}, f_{l_4}, f_{l_5}, f_{l_6}, f_{l_7}\}$
N_9	$\{f_{l_{10}}, f_{l_{11}}, \cdots, f_{l_{15}}, f_{l_{16}}, f_{l_{17}}, f_{l_{19}}\}$	$\{f_{l_9}\}$	$\{f_{l_1}, f_{l_2}, f_{l_3}, f_{l_4}, f_{l_5}, f_{l_6}, f_{l_7}, f_{l_8}\}$
N_{PLC}	$\{f_{l_{10}}, f_{l_{11}}, \cdots, f_{l_{15}}, f_{l_{16}}, f_{l_{17}}, f_{l_{18}}\}$	$\{f_{l_1}, f_{l_2}, f_{l_3}, f_{l_4}, f_{l_5}, f_{l_6}, f_{l_7}, f_{l_8}, f_{l_9}\}$	–

"–" denotes that the corresponding observation symptom is not significant

Table 3 Likelihoods of all the suspected IC faults contained in F_{R} in case study 1

f_j	f_{l_1}	f_{l_2}	f_{l_3}	f_{l_4}	f_{l_5}	f_{l_6}	f_{l_7}	f_{l_8}	f_{l_9}	$f_{l_{10}}$	$f_{l_{11}}$	$f_{l_{12}}$	$f_{l_{13}}$	$f_{l_{14}}$	$f_{l_{15}}$	$f_{l_{16}}$	$f_{l_{17}}$	$f_{l_{18}}$	$f_{l_{19}}$
$\mathfrak{C}_{f_j}$ ($\times 10^{-4}$)	**1083**	111	**1686**	33	616	1	**1716**	61	**1121**	28	45	55	86	12	**3216**	8	99	3	21

The values in bold represent the likelihood of the diagnosed IC fault

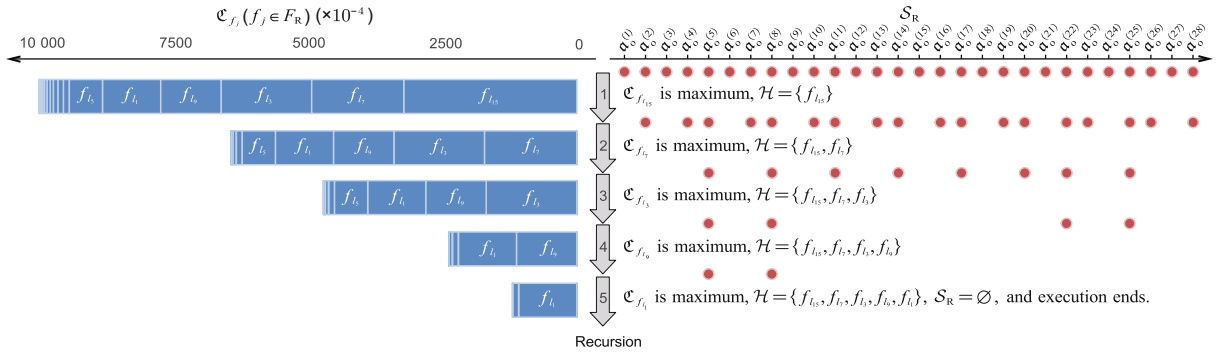

Fig. 6 Illustration of the algorithm execution process in case study 1

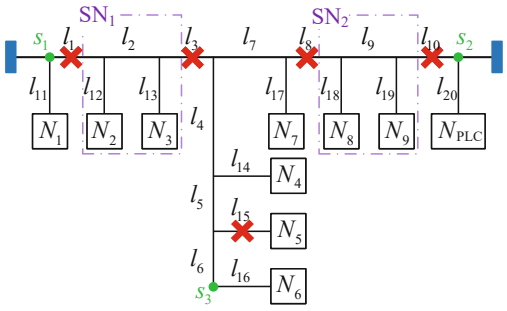

Fig. 7 Experimental setup in case study 2

branches. IC faults are independently injected into five cables: l_{15} has local IC faults at an injection rate of $\lambda_{\mathrm{IC}}^{l_{15}} = 1000$ faults/s, and l_1, l_3, l_8, and l_{10} have trunk IC faults at injection rates of $\lambda_{\mathrm{IC}}^{l_1} = 300$, $\lambda_{\mathrm{IC}}^{l_3} = 250$, $\lambda_{\mathrm{IC}}^{l_8} = 667$, and $\lambda_{\mathrm{IC}}^{l_{10}}$=667 faults/s. A total of 1700 error records are received in this case study.

The significant modes of the observation symptoms for all nodes as well as their quantities are shown in Table 4. Then, the set of observation symptoms can be expressed as $\mathcal{S}_{\mathrm{o}} = \{\mathfrak{a}_{N_1}^{<1>}, \mathfrak{a}_{N_1}^{<2>}, \mathfrak{a}_{N_1}^{<3>}, \mathfrak{a}_{N_2}^{<1>}, \cdots, \mathfrak{a}_{N_9}^{<4>}, \mathfrak{a}_{N_{\mathrm{PLC}}}^{<1>}, \mathfrak{a}_{N_{\mathrm{PLC}}}^{<2>}, \mathfrak{a}_{N_{\mathrm{PLC}}}^{<3>}\} = \{\mathfrak{a}_{\mathrm{o}}^{(u)} | u \in \{1, 2, \cdots, 34\}\}$.

Step 1: derive the set of suspected IC faults $\mathcal{F}_{\mathrm{o}}^{(u)}$ ($u \in \{1, 2, \cdots, 34\}$) for the corresponding observation symptom $\mathfrak{a}_{\mathrm{o}}^{(u)}$ by Eq. (2), as shown in Table 5.

Step 2: calculate the likelihood of all $f_j \in \bigcup_{v=1}^{34} \mathcal{F}_{\mathrm{o}}^{(v)}$ by Eq. (5), as shown in Table 6.

Step 3: determine the IC fault locations using Algorithm 1. The algorithm execution process is illustrated in Fig. 8, and the obtained set is $\mathcal{H} = \{f_{l_{15}}, f_{l_1}, f_{l_3}, f_{l_8}, f_{l_{10}}\}$. Hence, the determined IC faults are f_{l_1}, f_{l_3}, f_{l_8}, $f_{l_{10}}$, and $f_{l_{15}}$, which agrees with the experimental setup.

Table 4 Modes of observation symptoms and the corresponding quantities in case study 2

N_i	$t=1$		$t=2$		$t=3$		$t=4$	
	$\mathfrak{a}_{N_i}^{<t>}$	$\mathcal{Q}(\mathfrak{a}_{N_i}^{<t>})$	$\mathfrak{a}_{N_i}^{<t>}$	$\mathcal{Q}(\mathfrak{a}_{N_i}^{<t>})$	$\mathfrak{a}_{N_i}^{<t>}$	$\mathcal{Q}(\mathfrak{a}_{N_i}^{<t>})$	$\mathfrak{a}_{N_i}^{<t>}$	$\mathcal{Q}(\mathfrak{a}_{N_i}^{<t>})$
N_1	$(\mathbb{T},\mathbb{T},\mathbb{T})$	51	$(\mathbb{T},\mathbb{F},\mathbb{F})$	34	$(\mathbb{T},\mathbb{F},\mathbb{T})$	57	–	–
N_2	$(\mathbb{T},\mathbb{T},\mathbb{T})$	34	$(\mathbb{T},\mathbb{F},\mathbb{F})$	15	$(\mathbb{T},\mathbb{F},\mathbb{T})$	54	$(\mathbb{F},\mathbb{T},\mathbb{T})$	20
N_3	$(\mathbb{T},\mathbb{T},\mathbb{T})$	28	$(\mathbb{T},\mathbb{F},\mathbb{F})$	12	$(\mathbb{T},\mathbb{F},\mathbb{T})$	47	$(\mathbb{F},\mathbb{T},\mathbb{T})$	13
N_4	$(\mathbb{T},\mathbb{T},\mathbb{T})$	19	$(\mathbb{F},\mathbb{T},\mathbb{T})$	28	$(\mathbb{T},\mathbb{F},\mathbb{T})$	42	–	–
N_5	$(\mathbb{F},\mathbb{F},\mathbb{F})$	53	$(\mathbb{F},\mathbb{T},\mathbb{T})$	29	$(\mathbb{T},\mathbb{F},\mathbb{T})$	62	–	–
N_6	$(\mathbb{T},\mathbb{T},\mathbb{T})$	46	$(\mathbb{F},\mathbb{T},\mathbb{T})$	49	$(\mathbb{T},\mathbb{F},\mathbb{T})$	81	–	–
N_7	$(\mathbb{T},\mathbb{T},\mathbb{T})$	23	$(\mathbb{F},\mathbb{T},\mathbb{T})$	26	$(\mathbb{T},\mathbb{F},\mathbb{T})$	35	–	–
N_8	$(\mathbb{T},\mathbb{T},\mathbb{T})$	14	$(\mathbb{F},\mathbb{T},\mathbb{T})$	22	$(\mathbb{T},\mathbb{F},\mathbb{T})$	19	$(\mathbb{F},\mathbb{T},\mathbb{F})$	17
N_9	$(\mathbb{T},\mathbb{T},\mathbb{T})$	10	$(\mathbb{F},\mathbb{T},\mathbb{T})$	20	$(\mathbb{T},\mathbb{F},\mathbb{T})$	16	$(\mathbb{F},\mathbb{T},\mathbb{F})$	19
N_{PLC}	$(\mathbb{T},\mathbb{T},\mathbb{T})$	185	$(\mathbb{F},\mathbb{T},\mathbb{T})$	163	$(\mathbb{F},\mathbb{T},\mathbb{F})$	336	–	–

"–" denotes that the corresponding observation symptom is not significant

Table 5 Suspected IC fault sets of the corresponding observation symptoms in case study 2

N_i	$\mathcal{F}_{N_i}^{<1>}$	$\mathcal{F}_{N_i}^{<2>}$	$\mathcal{F}_{N_i}^{<3>}$	$\mathcal{F}_{N_i}^{<4>}$
N_1	$\{f_{l_{12}},f_{l_{13}},f_{l_{14}},f_{l_{15}},\cdots,f_{l_{20}}\}$	$\{f_{l_1},f_{l_2},f_{l_3}\}$	$\{f_{l_7},f_{l_8},f_{l_9},f_{l_{10}}\}$	–
N_2	$\{f_{l_{11}},f_{l_{13}},f_{l_{14}},f_{l_{15}},\cdots,f_{l_{20}}\}$	$\{f_{l_2},f_{l_3}\}$	$\{f_{l_7},f_{l_8},f_{l_9},f_{l_{10}}\}$	$\{f_{l_1}\}$
N_3	$\{f_{l_{11}},f_{l_{12}},f_{l_{14}},f_{l_{15}},\cdots,f_{l_{20}}\}$	$\{f_{l_3}\}$	$\{f_{l_7},f_{l_8},f_{l_9},f_{l_{10}}\}$	$\{f_{l_1},f_{l_2}\}$
N_4	$\{f_{l_{11}},f_{l_{12}},f_{l_{13}},f_{l_{15}},\cdots,f_{l_{20}}\}$	$\{f_{l_1},f_{l_2},f_{l_3}\}$	$\{f_{l_7},f_{l_8},f_{l_9},f_{l_{10}}\}$	–
N_5	$\{f_{l_{15}}\}$	$\{f_{l_1},f_{l_2},f_{l_3}\}$	$\{f_{l_7},f_{l_8},f_{l_9},f_{l_{10}}\}$	–
N_6	$\{f_{l_{11}},f_{l_{12}},\cdots,f_{l_{15}},f_{l_{17}},f_{l_{18}},f_{l_{19}},f_{l_{20}}\}$	$\{f_{l_1},f_{l_2},f_{l_3}\}$	$\{f_{l_7},f_{l_8},f_{l_9},f_{l_{10}}\}$	–
N_7	$\{f_{l_{11}},f_{l_{12}},\cdots,f_{l_{15}},f_{l_{16}},f_{l_{18}},f_{l_{19}},f_{l_{20}}\}$	$\{f_{l_1},f_{l_2},f_{l_3}\}$	$\{f_{l_8},f_{l_9},f_{l_{10}}\}$	–
N_8	$\{f_{l_{11}},f_{l_{12}},\cdots,f_{l_{15}},f_{l_{16}},f_{l_{17}},f_{l_{19}},f_{l_{20}}\}$	$\{f_{l_1},f_{l_2},f_{l_3}\}$	$\{f_{l_9},f_{l_{10}}\}$	$\{f_{l_7},f_{l_8}\}$
N_9	$\{f_{l_{11}},f_{l_{12}},\cdots,f_{l_{15}},f_{l_{16}},f_{l_{17}},f_{l_{18}},f_{l_{20}}\}$	$\{f_{l_1},f_{l_2},f_{l_3}\}$	$\{f_{l_{10}}\}$	$\{f_{l_7},f_{l_8},f_{l_9}\}$
N_{PLC}	$\{f_{l_{11}},f_{l_{12}},\cdots,f_{l_{15}},f_{l_{16}},f_{l_{17}},f_{l_{18}},f_{l_{19}}\}$	$\{f_{l_1},f_{l_2},f_{l_3}\}$	$\{f_{l_7},f_{l_8},f_{l_9},f_{l_{10}}\}$	–

"–" denotes that the corresponding observation symptom is not significant

Table 6 Likelihoods of all suspected IC faults contained in F_{R} in case study 2

f_j	f_{l_1}	f_{l_2}	f_{l_3}	f_{l_7}	f_{l_8}	f_{l_9}	$f_{l_{10}}$	$f_{l_{11}}$	$f_{l_{12}}$	$f_{l_{13}}$	$f_{l_{14}}$	$f_{l_{15}}$	$f_{l_{16}}$	$f_{l_{17}}$	$f_{l_{18}}$	$f_{l_{19}}$	$f_{l_{20}}$
$\mathfrak{C}_{f_j}$ $(\times10^{-4})$	**1961**	89	**1479**	90	**1474**	555	**1411**	4	28	8	1	**2879**	1	5	1	13	2

The values in bold represent the likelihood of the diagnosed IC fault

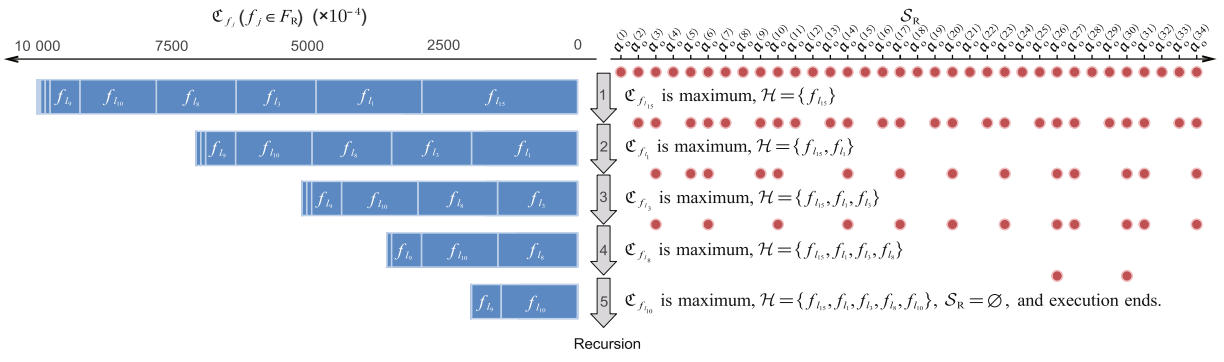

Fig. 8 Illustration of the algorithm execution process in case study 2

4.3 Case study 3: IC fault diagnosis for a five-branch complex topology network

In this case study, the network topology is shown in Fig. 9, which has 5 branches connecting 10 nodes. Four sensors s_1, s_2, s_3, s_4 are deployed at the ends of branches. IC faults are independently injected into four cables: l_{14} has local IC faults at an injection rate of $\lambda_{\text{IC}}^{l_{14}} = 667$ faults/s, and l_5, l_6, and l_7 have trunk IC faults at injection rates of $\lambda_{\text{IC}}^{l_5} = 250$, $\lambda_{\text{IC}}^{l_6} = 500$, and $\lambda_{\text{IC}}^{l_7} = 200$ faults/s. A total of 1074 error records are received in this case study.

The significant modes of the observation symptoms for all nodes as well as their quantities are shown in Table 7. Then, the set of observation symptoms can be expressed as $\mathcal{S}_{\mathrm{o}} = \{\mathfrak{a}_{N_1}^{<1>}, \mathfrak{a}_{N_1}^{<2>}, \mathfrak{a}_{N_2}^{<1>}, \cdots, \mathfrak{a}_{N_5}^{<3>}, \mathfrak{a}_{N_6}^{<1>}, \cdots, \mathfrak{a}_{N_{\mathrm{PLC}}}^{<2>}\} = \{\mathfrak{a}_{\mathrm{o}}^{(u)} | u \in \{1, 2, \cdots, 22\}\}$.

Step 1: derive the set of suspected IC faults $\mathcal{F}_{\mathrm{o}}^{(u)}$ ($u \in \{1, 2, \cdots, 22\}$) for the corresponding observation symptom $\mathfrak{a}_{\mathrm{o}}^{(u)}$ by Eq. (2), as shown in Table 8.

Step 2: calculate the likelihood of all $f_j \in \bigcup_{v=1}^{22} \mathcal{F}_{\mathrm{o}}^{(v)}$ by Eq. (5), as shown in Table 9.

Step 3: determine the IC fault locations using Algorithm 1. The algorithm execution process is illustrated in Fig. 10, and the obtained set is $\mathcal{H} = \{f_{l_{14}}, f_{l_6}, f_{l_7}, f_{l_5}\}$. Hence, the determined IC faults are f_{l_5}, f_{l_6}, f_{l_7}, and $f_{l_{14}}$, which agrees with the experimental setup.

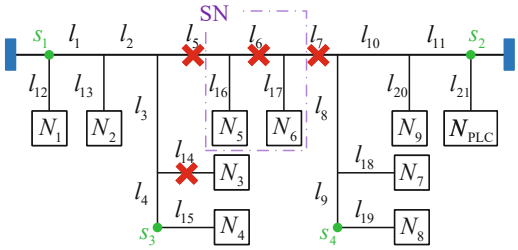

Fig. 9 Experimental setup in case study 3

5 Discussion

In this section, the method proposed in this work is compared to state-of-the-art IC fault diagnosis methods in Zhang et al. (2017, 2019) and Wang LK et al. (2023) to demonstrate the advantages and performance improvements of this work. Based on the same network topology and the same setup of fault locations, the IC fault locations diagnosed using

Table 7 Modes of observation symptoms and the corresponding quantities in case study 3

N_i	$t=1$		$t=2$		$t=3$	
	$\mathfrak{a}_{N_i}^{<t>}$	$\mathcal{Q}(\mathfrak{a}_{N_i}^{<t>})$	$\mathfrak{a}_{N_i}^{<t>}$	$\mathcal{Q}(\mathfrak{a}_{N_i}^{<t>})$	$\mathfrak{a}_{N_i}^{<t>}$	$\mathcal{Q}(\mathfrak{a}_{N_i}^{<t>})$
N_1	$(\mathbb{T}, \mathbb{T}, \mathbb{T}, \mathbb{T})$	29	$(\mathbb{T}, \mathbb{F}, \mathbb{T}, \mathbb{F})$	39	–	–
N_2	$(\mathbb{T}, \mathbb{T}, \mathbb{T}, \mathbb{T})$	20	$(\mathbb{T}, \mathbb{F}, \mathbb{T}, \mathbb{F})$	48	–	–
N_3	$(\mathbb{F}, \mathbb{F}, \mathbb{F}, \mathbb{F})$	30	$(\mathbb{T}, \mathbb{F}, \mathbb{T}, \mathbb{F})$	54	–	–
N_4	$(\mathbb{T}, \mathbb{T}, \mathbb{T}, \mathbb{T})$	23	$(\mathbb{T}, \mathbb{F}, \mathbb{T}, \mathbb{F})$	39	–	–
N_5	$(\mathbb{T}, \mathbb{T}, \mathbb{T}, \mathbb{T})$	19	$(\mathbb{T}, \mathbb{F}, \mathbb{T}, \mathbb{F})$	35	$(\mathbb{F}, \mathbb{T}, \mathbb{F}, \mathbb{T})$	11
N_6	$(\mathbb{T}, \mathbb{T}, \mathbb{T}, \mathbb{T})$	15	$(\mathbb{T}, \mathbb{F}, \mathbb{T}, \mathbb{F})$	8	$(\mathbb{F}, \mathbb{T}, \mathbb{F}, \mathbb{T})$	24
N_7	$(\mathbb{T}, \mathbb{T}, \mathbb{T}, \mathbb{T})$	29	$(\mathbb{F}, \mathbb{T}, \mathbb{F}, \mathbb{T})$	56	–	–
N_8	$(\mathbb{T}, \mathbb{T}, \mathbb{T}, \mathbb{T})$	31	$(\mathbb{F}, \mathbb{T}, \mathbb{F}, \mathbb{T})$	57	–	–
N_9	$(\mathbb{T}, \mathbb{T}, \mathbb{T}, \mathbb{T})$	15	$(\mathbb{F}, \mathbb{T}, \mathbb{F}, \mathbb{T})$	47	–	–
N_{PLC}	$(\mathbb{T}, \mathbb{T}, \mathbb{T}, \mathbb{T})$	154	$(\mathbb{F}, \mathbb{T}, \mathbb{F}, \mathbb{T})$	274	–	–

"–" denotes that the corresponding observation symptom is not significant

Table 8 Suspected IC fault sets of the corresponding observation symptoms in case study 3

N_i	$\mathcal{F}_{N_i}^{<1>}$	$\mathcal{F}_{N_i}^{<2>}$	$\mathcal{F}_{N_i}^{<3>}$
N_1	$\{f_{l_{13}}, f_{l_{14}}, f_{l_{15}}, f_{l_{16}}, f_{l_{17}}, f_{l_{18}}, f_{l_{19}}, f_{l_{20}}, f_{l_{21}}\}$	$\{f_{l_5}, f_{l_6}, f_{l_7}\}$	–
N_2	$\{f_{l_{12}}, f_{l_{14}}, f_{l_{15}}, f_{l_{16}}, f_{l_{17}}, f_{l_{18}}, f_{l_{19}}, f_{l_{20}}, f_{l_{21}}\}$	$\{f_{l_5}, f_{l_6}, f_{l_7}\}$	–
N_3	$\{f_{l_{14}}\}$	$\{f_{l_5}, f_{l_6}, f_{l_7}\}$	–
N_4	$\{f_{l_{12}}, f_{l_{13}}, f_{l_{14}}, f_{l_{16}}, f_{l_{17}}, f_{l_{18}}, f_{l_{19}}, f_{l_{20}}, f_{l_{21}}\}$	$\{f_{l_5}, f_{l_6}, f_{l_7}\}$	–
N_5	$\{f_{l_{12}}, f_{l_{13}}, f_{l_{14}}, f_{l_{15}}, f_{l_{17}}, f_{l_{18}}, f_{l_{19}}, f_{l_{20}}, f_{l_{21}}\}$	$\{f_{l_6}, f_{l_7}\}$	$\{f_{l_5}\}$
N_6	$\{f_{l_{12}}, f_{l_{13}}, f_{l_{14}}, f_{l_{15}}, f_{l_{16}}, f_{l_{18}}, f_{l_{19}}, f_{l_{20}}, f_{l_{21}}\}$	$\{f_{l_7}\}$	$\{f_{l_5}, f_{l_6}\}$
N_7	$\{f_{l_{12}}, f_{l_{13}}, f_{l_{14}}, f_{l_{15}}, f_{l_{16}}, f_{l_{17}}, f_{l_{19}}, f_{l_{20}}, f_{l_{21}}\}$	$\{f_{l_5}, f_{l_6}, f_{l_7}\}$	–
N_8	$\{f_{l_{12}}, f_{l_{13}}, f_{l_{14}}, f_{l_{15}}, f_{l_{16}}, f_{l_{17}}, f_{l_{18}}, f_{l_{20}}, f_{l_{21}}\}$	$\{f_{l_5}, f_{l_6}, f_{l_7}\}$	–
N_9	$\{f_{l_{12}}, f_{l_{13}}, f_{l_{14}}, f_{l_{15}}, f_{l_{16}}, f_{l_{17}}, f_{l_{18}}, f_{l_{19}}, f_{l_{21}}\}$	$\{f_{l_5}, f_{l_6}, f_{l_7}\}$	–
N_{PLC}	$\{f_{l_{12}}, f_{l_{13}}, f_{l_{14}}, f_{l_{15}}, f_{l_{16}}, f_{l_{17}}, f_{l_{18}}, f_{l_{19}}, f_{l_{20}}\}$	$\{f_{l_5}, f_{l_6}, f_{l_7}\}$	–

"–" denotes that the corresponding observation symptom is not significant

Table 9 Likelihoods of all the suspected IC faults contained in F_{R} in case study 3

f_j	f_{l_5}	f_{l_6}	f_{l_7}	$f_{l_{12}}$	$f_{l_{13}}$	$f_{l_{14}}$	$f_{l_{15}}$	$f_{l_{16}}$	$f_{l_{17}}$	$f_{l_{18}}$	$f_{l_{19}}$	$f_{l_{20}}$	$f_{l_{21}}$
$\mathfrak{C}_{f_j}$ ($\times 10^{-4}$)	**787**	**3349**	**1319**	17	20	**4020**	143	18	107	56	48	44	74

The values in bold represent the likelihood of the diagnosed IC fault

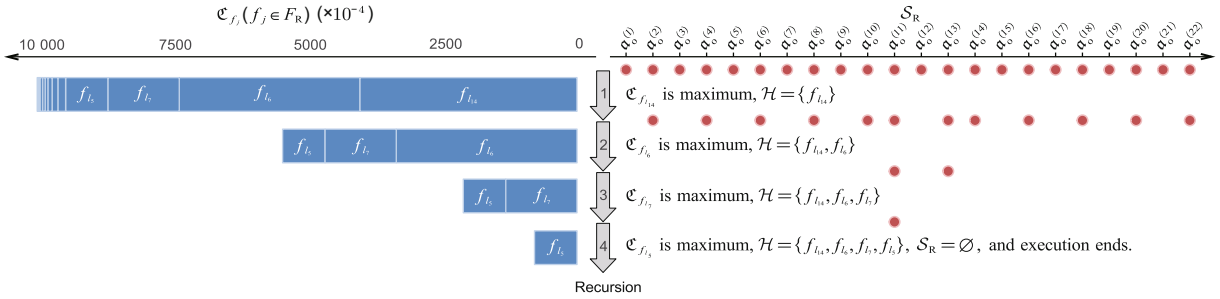

Fig. 10 Illustration of the algorithm execution process in case study 3

Table 10 Comparison of the IC fault diagnosis results and performance of existing methods

Method	Case study 1				Case study 2				Case study 3				Practicability	Complexity
	Ω_*	FNR	FPR	EFF	Ω_*	FNR	FPR	EFF	Ω_*	FNR	FPR	EFF		
Zhang et al. (2017)'s	$\{l_1,l_9,l_{15}\}$	40%	**0**	0	$\{l_1,l_4,l_5,l_{10},l_{15}\}$	40%	13%	0	$\{l_3,l_5,l_7,l_{14}\}$	25%	6%	0	⩒	
Zhang et al. (2019)'s	$\{l_1,l_9,l_{15}\}$	40%	**0**	0	$\{l_1,l_4,l_5,l_{10},l_{15}\}$	40%	13%	0	$\{l_3,l_5,l_7,l_{14}\}$	25%	6%	0	⩒	
Wang LK et al. (2023)'s	$\{l_1,l_3,l_7,l_9,l_{15}\}$	**0**	**0**	33%	$\{l_1,l_2,l_3,l_8,l_9,l_{10},l_{15}\}$	**0**	13%	0	$\{l_5,l_6,l_7,l_{14}\}$	**0**	**0**	50%	⩓	⩓
Ours	$\{l_1,l_3,l_7,l_9,l_{15}\}$	**0**	**0**	**100%**	$\{l_1,l_3,l_8,l_{10},l_{15}\}$	**0**	**0**	**100%**	$\{l_5,l_6,l_7,l_{14}\}$	**0**	**0**	**100%**	⩒	⩒

The best results are in bold. ⩒ and ⩓ mean good and poor results, respectively

different methods along with various diagnostic performance indexes are shown in Table 10, and the details are introduced in this section.

5.1 Localization accuracy

To evaluate the accuracy of the diagnosis results, we quantitatively evaluate two diagnosis errors, missed diagnosis and misdiagnosis, using the false negative rate (FNR) and false positive rate (FPR), respectively, which are calculated as

$$\mathrm{FNR}=\frac{\#(\Omega-\Omega_*)}{\#(\Omega)}\times 100\%,$$
$$\mathrm{FPR}=\frac{\#(\Omega_*-\Omega)}{\#(\Omega^{\mathrm{c}})}\times 100\%,$$

where $\#(\cdot)$ is the cardinality of set $\cdot$, Ω is the set of actual fault locations, Ω_* is the set of diagnosed fault locations, and Ω^{c} is the complement of set Ω, that is, the set of fault-free locations.

The diagnosis errors of different methods in the three case studies are shown in Table 10 and can be summarized as follows: Existing methods have various degrees of misdiagnosis and missed diagnosis under different network topologies and fault location setups, and the diagnosis errors all appear within the non-diagnosable subnets. This is because existing methods rely only on the information about the significance distribution of observation symptoms to roughly estimate the occurrence probability of each suspected IC fault. However, the significance distribution of the symptoms depends on the locations of the two most marginal trunk faults within the same branch, that is, the non-diagnosable subnet. Thus, whether faults occur within the non-diagnosable subnet does not change the significance distribution of symptoms; that is, existing distribution-based qualitative diagnostic strategies cannot correctly diagnose the faults within the non-diagnosable subnets.

In contrast, both the FNR and FPR of the proposed method are zero, which indicates that the fault locations can be identified completely and accurately in different complex fault scenarios. This is because considering that the occurrence or non-occurrence of a fault within the non-diagnosable subnet causes a change in the number of some observation symptoms, the proposed method exploits the exact probability of each suspected IC fault calculated based on the

number of symptoms to identify the faults within the non-diagnosable subnet, which allows the proposed method to accurately diagnose all IC faults in the network. Therefore, the method proposed in this work represents an improvement over existing methods in terms of localization accuracy.

In addition, it is worth mentioning that the localization accuracy of the proposed method may be affected by the distribution of fault rates. Based on case study 1, we adjust the injection rates of IC faults to $\lambda_{\mathrm{IC}}^{l_{15}}=300$, $\lambda_{\mathrm{IC}}^{l_1}=667$, $\lambda_{\mathrm{IC}}^{l_3}=250$, $\lambda_{\mathrm{IC}}^{l_7}=500$, and $\lambda_{\mathrm{IC}}^{l_9}=1000$ faults/s and then apply the proposed method for diagnosis. The observation symptom modes and the suspected IC fault sets are the same in case study 1, and the likelihoods of the suspected IC faults are shown in Table 11. The identified fault locations are f_{l_1}, f_{l_7}, f_{l_9}, and $f_{l_{15}}$, while f_{l_3} is missed. This is because f_{l_1} and f_{l_7}, which have greater likelihoods than f_{l_3}, are prioritized for diagnosis over f_{l_3}, and the suspected IC fault sets containing f_{l_1} or f_{l_7} must contain f_{l_3}, so f_{l_3} is missed. The low likelihood of f_{l_3} is strongly related to the low rate of faults. Hence, it can be concluded that the proposed method may not be able to diagnose the trunk IC fault whose rate is much lower than the rates of the trunk IC faults on both sides of it, and we will explore more accurate diagnosis methods for this very slow middle and very fast side fault scenarios in future work.

5.2 Diagnostic efficiency

In this paper, we quantitatively assess the efficiency (EFF) of a diagnosis method using the number of diagnostic rounds required to locate all IC faults, where a diagnostic round includes installing sensors, processing data, and executing algorithms. The efficiency is calculated as follows:

$$\mathrm{EFF}=\frac{1}{N_{\mathrm{r}}}\times 100\%,$$

where N_{r} is the number of diagnostic rounds. Table 10 shows the efficiency of different methods in the three case studies, and their calculations are detailed as follows:

Based on the discussion in Section 5.1, the existing methods are unable to correctly determine the health of the cables within the non-diagnosable subnets, and thus the non-diagnosable subnets need to be additionally diagnosed. Because Zhang et al. (2017, 2019) did not analyze diagnosability and did not diagnose non-diagnosable subnets, they are unable to locate all faults, and the number of diagnostic rounds can be considered as $N_{\mathrm{r}}=\infty$. Therefore, the efficiency of both methods is $\mathrm{EFF}=\frac{1}{\infty}\times 100\%=0$. In contrast, in Wang LK et al. (2023), the diagnostic framework was divided into two parts, the initial diagnosis of the whole network and the diagnosis of the non-diagnosable subnets one by one. For example, in case study 3, Wang LK et al. (2023) located the faults f_{l_5}, f_{l_7}, and $f_{l_{14}}$ in the first diagnostic round, determined a non-diagnosable subnet between f_{l_5} and f_{l_7}, as the area SN shown in Fig. 9, and performed the second round on the subnet SN, which identifies the IC fault f_{l_6}. Thus, the diagnostic round in case study 3 is $N_{\mathrm{r}}=2$, and the efficiency is $\mathrm{EFF}=\frac{1}{2}\times 100\%=50\%$. As another example, the first round in case study 1 identifies the non-diagnosable subnet SN_1 in Fig. 5, the second round identifies the subnet SN_2, and the third round determines that the links within SN_2 are fault-free; thus, $N_{\mathrm{r}}=3$ and $\mathrm{EFF}=\frac{1}{3}\times 100\%=33\%$ for case study 1. In case study 2, the efficiency of Wang LK et al. (2023) was $\mathrm{EFF}=\frac{1}{\infty}\times 100\%=0$ due to misdiagnosis.

In contrast, the method proposed in this work exploits the exact posterior probability of each suspected IC fault to determine the IC fault locations, which allows the proposed framework to localize all IC faults after one diagnostic round without the need for repeated diagnosis of the non-diagnosable subnets. Therefore, the efficiency of the proposed method is $\mathrm{EFF}=100\%$ for the three case studies, which indicates that the proposed method presents an improvement over existing methods in terms of diagnostic efficiency.

In addition, note that throughout the diagnostic

Table 11 Likelihoods of the suspected IC faults in the case study in Section 5.1

f_j	f_{l_1}	f_{l_2}	f_{l_3}	f_{l_4}	f_{l_5}	f_{l_6}	f_{l_7}	f_{l_8}	f_{l_9}	$f_{l_{10}}$	$f_{l_{11}}$	$f_{l_{12}}$	$f_{l_{13}}$	$f_{l_{14}}$	$f_{l_{15}}$	$f_{l_{16}}$	$f_{l_{17}}$	$f_{l_{18}}$	$f_{l_{19}}$
$\mathfrak{C}_{f_j}$ ($\times 10^{-4}$)	**1497**	23	958	10	467	159	**2132**	371	**811**	311	89	12	9	127	**1948**	323	423	164	166

The values in bold represent the likelihood of the diagnosed IC fault

process, the proposed method needs only to attach the sensor to the end of the network to achieve the complete diagnosability of a network; the end of the network commonly has open ports to facilitate hookup of external devices, whereas in Wang LK et al. (2023), diagnosing the non-diagnosable subnets requires re-configuration of the sensor layout and repeatedly hooking up and removing the sensors inside the network. However, the interior of DeviceNet is generally not directly accessible. Therefore, we can conclude that the method proposed in this work has an advantage over existing methods in terms of practical engineering implementation.

Moreover, the diagnostic speed of the proposed data-driven method is analyzed from the perspective of data size required for accurate diagnosis, because time is mainly consumed in collecting data. Using three data sizes, we repeated 300 groups of experiments for each case study to obtain the means and standard deviations of diagnostic errors. As shown in Fig. 11, the diagnostic errors in all cases are quite large if the data size is less than 1000, and the diagnostic errors can uniformly stabilize below 1% if the data size reaches 1000. Hence, as a rule of thumb, the proposed method is sufficient to accurately identify IC faults when the data size reaches 1000.

5.3 Algorithm complexity

Considering that Zhang et al. (2017, 2019) did not correctly diagnose the faults in complex topologies, we compare the complexity of the MLBFD algorithm proposed in this work with the filtered search algorithm (FSA) (Wang LK et al., 2023). Both the MLBFD algorithm and FSA select the faults with the highest probability among the remaining suspected IC faults and iteratively update the set of determined IC faults, until all observation symptoms have been explained. However, because the two methods calculate the probability of faults in different ways, the number of faults with the highest probability in a single search process is different,

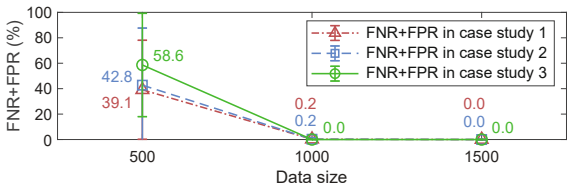

Fig. 11 Trends in diagnostic errors of the proposed method versus data size

and then the number of search process executions is different.

In Wang LK et al. (2023), the probability of a suspected IC fault is essentially the proportion of the suspected IC faults to the suspected IC faults of all nodes. Because a trunk fault on the left (right) side of a node causes all trunk lines on its left (right) side to be derived as suspected IC faults, the suspected IC faults of the nodes between two trunk faults are the same. In this way, the probabilities of suspected IC faults between trunk faults are the same, and the number of these suspected IC faults is the number of search process executions in the next layer. Thus, the computational complexity of FSA is $O_{\mathrm{FSA}}=O(\sum_{i=1}^{n}(c_i+b_i^{2,\mathrm{c}}(c_i-1)+b_i^{3,\mathrm{c}}(c_i-2)+\cdots+0+g_i+b_i^{2,\mathrm{g}}(g_i-1)+b_i^{3,\mathrm{g}}(g_i-2)+\cdots+0))\geq O(c_1+(c_1-1)+(c_1-2)+\cdots+0+g_1+(g_1-1)+(g_1-2)+\cdots+0)$, where n is the number of iterative updates of the determined IC fault set, c_i and g_i are the numbers of drop and trunk lines in the i^{th} update process, respectively, and $b_i^{m,\mathrm{c}}$ and $b_i^{m,\mathrm{g}}$ are the numbers of local and trunk IC fault sequences of level m ($m\geq 2$) in the i^{th} update process, respectively.

In contrast, the method proposed in this work accurately calculates the posterior probability of each suspected IC fault occurring in the network based on the quantity of each observation symptom. Thus, the probability of each suspected IC fault differs depending on the quantity of the corresponding symptoms, and then an IC fault consumes only one search process. Thus, the computational complexity of the MLBFD algorithm is $O_{\mathrm{MLBFD}}=O((c_1+g_1)+(c_1-d_1^{\mathrm{c}}+g_1-d_1^{\mathrm{g}})+(c_1-d_1^{\mathrm{c}}-d_2^{\mathrm{c}}+g_1-d_1^{\mathrm{g}}-d_2^{\mathrm{g}})+\cdots+0)\leq O((c_1+g_1)+(c_1-1+g_1-1)+(c_1-2+g_1-2)+\cdots+0)\leq O_{\mathrm{FSA}}$, where d_p^{c} and d_p^{g} are the numbers of local and trunk IC faults deleted in the p^{th} update process, respectively. Then considering case study 1 as an example, the computational complexity of FSA is $O((10+9+9\times 8)+(7+5\times 6))=O(128)$, whereas it is $O((10+9)+9+8+4+2)=O(42)$ for the MLBFD algorithm. Therefore, the proposed method has an advantage over existing methods in terms of algorithm complexity.

6 Conclusions

In this paper, we propose a novel data-driven IC fault diagnosis method based on Bayesian inference

for DeviceNet with complex topological layouts. The observation symptoms are produced by the sensors deployed at each branch end of the network. The suspected IC faults for the observation symptoms are derived and the fault likelihoods are calculated using the Bayesian inference approach. The maximum likelihood-based fast diagnosis algorithm is developed based on the above three parameters to accurately and efficiently diagnose all IC faults in a network. The testbed is constructed and case studies are performed to demonstrate and evaluate the proposed method. The experimental results show that the IC fault locations diagnosed by the proposed method agree well with the experiment setup in various complex topologies and fault scenarios. Further discussion shows that the proposed method is an improvement over existing methods in terms of localization accuracy, diagnostic efficiency, practicality, and algorithm complexity.

Future work will include improving the robustness of the current method to variations in the rate distribution of IC faults and extending the current method to the short-circuit IC fault scenario.

Contributors

Longkai WANG and Yong LEI designed the research. Longkai WANG processed the data and drafted the paper. Yong LEI helped organize the paper. Longkai WANG revised and finalized the paper.

Conflict of interest

Both authors declare that they have no conflict of interest.

Data availability

The data that support the findings of this study are available from the corresponding author upon reasonable request.

References

Cai BP, Huang L, Xie M, 2017. Bayesian networks in fault diagnosis. *IEEE Trans Ind Inform*, 13(5):2227-2240. https://doi.org/10.1109/TII.2017.2695583

Cheng S, Peng HN, Yang C, et al., 2024a. Chassis global dynamics optimization for automated vehicles: a multi-actuator integrated control method. *IEEE Trans Syst Man Cybern Syst*, 54(1):578-587. https://doi.org/10.1109/TSMC.2023.3311446

Cheng S, Peng HN, Dong XX, et al., 2024b. Chassis global dynamics-oriented trajectory planning for automated vehicles. *IEEE Trans Syst Man Cybern Syst*, 54(2):950-959. https://doi.org/10.1109/TSMC.2023.3321881

Chu KY, Liu R, Duan GJ, 2023. A gray correlation based Bayesian network model for fault source diagnosis of multistage process—small sample manufacturing system. *Adv Eng Inform*, 56:101918. https://doi.org/10.1016/j.aei.2023.101918

Gessner D, Barranco M, Ballesteros A, et al., 2014. sfiCAN: a star-based physical fault-injection infrastructure for CAN networks. *IEEE Trans Veh Technol*, 63(3):1335-1349. https://doi.org/10.1109/TVT.2013.2284030

Jiang XJ, Zhou W, Hou J, 2023. Construction of fault diagnosis system for control rod drive mechanism based on knowledge graph and Bayesian inference. *Nucl Sci Techn*, 34:21. https://doi.org/10.1007/s41365-023-01173-8

Lei Y, Yuan Y, Sun YC, 2014a. Fault location identification for localized intermittent connection problems on CAN networks. *Chin J Mech Eng*, 27(5):1038-1046. https://doi.org/10.3901/CJME.2014.0527.301

Lei Y, Yuan Y, Zhao JZ, 2014b. Model-based detection and monitoring of the intermittent connections for CAN networks. *IEEE Trans Ind Electron*, 61(6):2912-2921. https://doi.org/10.1109/TIE.2013.2272277

Lei Y, Xie HB, Yuan Y, et al., 2015. Fault location for the intermittent connection problems on CAN networks. *IEEE Trans Ind Electron*, 62(11):7203-7213. https://doi.org/10.1109/TIE.2015.2442518

Liu BY, Bi XW, Gu LJ, et al., 2022. Application of a Bayesian network based on multi-source information fusion in the fault diagnosis of a radar receiver. *Sensors*, 22(17):6396. https://doi.org/10.3390/s22176396

Liu ZK, Lv KL, Zheng C, et al., 2022. A fault diagnosis method for rolling element bearings based on ICEEMDAN and Bayesian network. *J Mech Sci Technol*, 36(5):2201-2212. https://doi.org/10.1007/s12206-022-0404-3

Nguyen TN, Vilim RB, 2023. Direct Bayesian inference for fault severity assessment in digital-twin-based fault diagnosis. *Ann Nucl Energy*, 194:109932. https://doi.org/10.1016/j.anucene.2023.109932

Open DeviceNet Vendor Association, 2021. Technology Overview Series: DeviceNet.

Wang LK, Zhang LM, Lei Y, 2023. Diagnosis of intermittent connection faults for CAN networks with complex topology. *IEEE Access*, 11:52199-52213. https://doi.org/10.1109/ACCESS.2023.3278105

Wang ZW, Wang L, Tan YY, et al., 2021. Fault diagnosis using fused reference model and Bayesian network for building energy systems. *J Build Eng*, 34:101957. https://doi.org/10.1016/j.jobe.2020.101957

Yang C, Cai BP, Zhang R, et al., 2023a. Cross-validation enhanced digital twin driven fault diagnosis methodology for minor faults of subsea production control system. *Mech Syst Signal Process*, 204:110813. https://doi.org/10.1016/j.ymssp.2023.110813

Yang C, Cai BP, Wu QB, et al., 2023b. Digital twin-driven fault diagnosis method for composite faults by combining virtual and real data. *J Ind Inform Integr*, 33:100469. https://doi.org/10.1016/j.jii.2023.100469

Yang WT, Reis MS, Borodin V, et al., 2022. An interpretable unsupervised Bayesian network model for fault detection and diagnosis. *Contr Eng Pract*, 127:105304. https://doi.org/10.1016/j.conengprac.2022.105304

Zhang LM, Lei Y, Chang Q, 2017. Intermittent connection fault diagnosis for CAN using data link layer information. *IEEE Trans Ind Electron*, 64(3):2286-2295. https://doi.org/10.1109/TIE.2016.2624261

Zhang LM, Yang F, Lei Y, 2019. Tree-based intermittent connection fault diagnosis for controller area network. *IEEE Trans Veh Technol*, 68(9):9151-9161. https://doi.org/10.1109/TVT.2019.2929419

Zhao JZ, Lei Y, 2012. Modeling for early fault detection of intermittent connections on controller area networks. IEEE/ASME Int Conf on Advanced Intelligent Mechatronics, p.1135-1140. https://doi.org/10.1109/AIM.2012.6265905